



Published in final edited form as:

Semin Nucl Med. 2010 May ; 40(3): 167–181. doi:10.1053/j.semnuclmed.2009.12.005.

Novel Antibody Vectors for Imaging

Tove Olafsen, Ph.D.[‡] and Anna M. Wu, Ph.D.

UCLA Crump Institute for Molecular Imaging, Department of Molecular and Medical Pharmacology, David Geffen School of Medicine, University of California at Los Angeles, Los Angeles, California

Abstract

Non-invasive molecular imaging approaches include nuclear, optical, MRI, CT, ultrasound and photoacoustic imaging, which require accumulation of a signal delivered by a probe at the target site. Monoclonal antibodies (mAbs) are high affinity molecules that can be used for specific, high signal delivery to cell surface molecules. However, their long circulation time in blood makes them unsuitable as imaging probes. Efforts to improve antibodies pharmacokinetics without compromising affinity and specificity have been made through protein engineering. Antibody variants that differ in antigen binding sites and size have been generated and evaluated as imaging probes to target tissues of interest. Fast clearing fragments such as single-chain Fv (scFv; 25 kDa) with one antigen binding site (monovalent) demonstrated low accumulation in tumors due to the low exposure time to the target. Using scFv as building block to produce larger, bivalent fragments such as scFv dimers (diabodies, 50 kDa) and scFv-fusion proteins (80 kDa minibodies and 105 kDa scFv-Fc) resulted in higher tumor accumulation due to their longer residence time in blood. Imaging studies with these fragments following radiolabeling have demonstrated excellent, high contrast images in gamma cameras and PET scanners. Several studies have also investigated antibody fragments conjugated to fluorescence (near infrared dyes), bioluminescence (luciferases) and quantum dots for optical imaging and iron oxides nanoparticles for MRI. However, these studies indicate that there are several factors that influence successful targeting and imaging. These include stability of the antibody fragment, the labeling chemistry (direct or indirect), whether critical residues are modified, the number of antigen expressed on the cell, and whether the target has a rapid recycling rate or internalizes upon binding. The preclinical data presented are compelling and it is evident that antibody-based molecular imaging tracers will play an important future role in the diagnosis and management of cancer and other diseases.

INTRODUCTION

Monoclonal antibodies (mAbs) have long been considered attractive candidates for targeted therapy and diagnostics due to their highly specific targeting ability. However, despite considerable efforts in developing mAb-based therapeutics for more than 30 years, initial progress was slow because poor performance of rodent mAbs in humans [i.e. human anti-mouse antibody (HAMA) responses, short half-lives and inability to trigger human effector functions]. With the advances in protein engineering techniques, genetics and proteomics, the

© 2009 Elsevier Inc. All rights reserved.

[‡]To whom correspondence should be addressed; Tove Olafsen, UCLA Crump Institute for Molecular Imaging, California NanoSystems Institute, room 4350B, 570 Westwood Plaza, Building 114, Box 951770, Los Angeles, CA 90095-1770, USA. Phone; 310-983-3198; Fax: 319-206-8975; tolafsen@mednet.ucla.edu.

Publisher's Disclaimer: This is a PDF file of an unedited manuscript that has been accepted for publication. As a service to our customers we are providing this early version of the manuscript. The manuscript will undergo copyediting, typesetting, and review of the resulting proof before it is published in its final citable form. Please note that during the production process errors may be discovered which could affect the content, and all legal disclaimers that apply to the journal pertain.

pharmaceutical industry has embraced mAbs as a new group of targeted drugs which has led to numerous FDA approved therapeutic mAbs.

For diagnostic imaging, only a handful of mAbs have been approved in the United States for single photon emission computed tomography (SPECT) imaging (Table 1). Most of these are no longer marketed in the US; only ProstaScint, LeukoScan, Bexxar and Zevalin are currently used in the clinic. Since these imaging agents are derived from murine mAbs, repeated use in humans limited except in patients with low grade B-cell lymphomas; a disease characterized by reduced host-immune recognition. In addition to straight diagnostic applications, antibody imaging can provide targeting and dosimetry information that can guide therapy. For example, both ^{131}In -labeled Bexxar and ^{111}In -labeled Zevalin can be used in combination with ^{90}Y and ^{131}I radioimmunotherapy, respectively, in patients with B-cell lymphomas. Image-guided therapies would be beneficial to other malignancies as well, and antibodies, due to their biological specificity, continue to be a promising avenue for developing new imaging probes for targeted treatment planning and monitoring.

The discipline of molecular imaging is one of the most rapidly growing areas of science. It offers the ability to visualize, characterize and measure processes on molecular and cellular levels non-invasively in living systems. The key players for obtaining this information are the molecular imaging agent (probe or tracer) and the target which can be intracellular or cell surface proteins. Radiolabeled probes for SPECT or positron emission tomography (PET), offer visualization of physiological and biochemical changes. Conventional imaging modalities on the other hand [radiography, ultrasonography (US), computed tomography (CT) and magnetic resonance imaging (MRI)], offer visualization of non-specific changes related to morphology. PET is a highly sensitive radiotracer imaging modality with only 10^{-11} – 10^{-12} mol/L levels of probe required for detection ¹. Although numerous tracers for imaging cancers by PET have been developed, only the glucose analogue [^{18}F]fluoro-2-*D*-deoxyglucose (FDG) which is a substrate for hexokinase in glucose metabolism, and [^{18}F] fluoride ions such as ^{18}F - NaF_2 for bone imaging (incorporated in the hydroxyapatite crystals in bone) are approved by FDA as PET probes. The major issues associated with FDG are non-specific and elevated uptake in inflammatory or infectious lesions, and variable physiological uptakes in normal tissues/organs that can be confused with malignant neoplasm ². In addition, lack of uptake in metabolically inactive malignant tissues will fail to be detected by FDG-PET. One approach to overcome the limitations of FDG-PET is to use targeting molecules/ligands that can specifically localize to cell-surface markers such as growth factor receptors, adhesion molecules, and differentiation and activation markers. Targets that have been subjected to intense research for oncological molecular imaging include angiogenesis ³, apoptosis ⁴, signal transduction and protein interaction networks ⁵, receptor- or enzyme-based ^{6, 7} and metabolic imaging ⁸ as well as inquiries about multidrug-resistance ^{9, 10} and gene delivery and expression ¹¹. Identification and validation of novel molecular markers have introduced several new targeted drugs into the clinic. Additionally, technical advances in instrumentation have enabled the combination of anatomy and molecular events into a single image through fused imaging modalities such as PET/CT, PET/MRI and SPECT/CT.

Today's antibody engineering technologies enable routine production of novel fully human or humanized mAbs from display libraries or from immunized transgenic mice carrying human immunoglobulin genes. Despite the development of non-immunogenic antibodies, only HumaSPECT (not approved in US) is human amongst the diagnostic mAbs/Fab listed in Table 1. A major disadvantage of using intact antibodies as imaging probes is that they circulate in the blood for several days. Early studies of antibody-based imaging agents showed that blood clearance was inversely related to the size of the protein i.e. clearance rate of Fab or Fab' > F(ab')₂ > IgG ^{12, 13}. For this reason Fab fragments, produced by proteolytic digested mAbs were developed into imaging agents (Table 1). However, the disadvantage of this fragment is that

it has only one antigen binding site (monovalent), which reduces the overall functional affinity (avidity) of the antibody. The production of genetically engineered antibody fragments of different sizes and valencies started with the introduction of a single-chain variable fragment (scFv, 25 kDa) (Figure 1) ^{14, 15}. Using scFv as building block, larger antibody fragments such as diabodies (dimers of scFv, 50 kDa), minibodies (dimers of scFv-C_H3, 80 kDa) and scFv-Fc dimers (105 kDa) have been generated (Figure 1) ¹⁶. These fragments have exhibited better tumor penetration, faster clearance kinetics and excellent tumor to blood ratios, which are desirable properties for an imaging probe. The blood clearance and tumor uptake curves of radioiodinated anti-carcinoembryonic antigen (CEA) scFv, diabody, minibody and a rapid clearing scFv-Fc fragment are shown in Figure 2. The rapid elimination has been attributed to their size and lack of interaction with the neonatal Fc receptor (FcRn).

Once the optimal antibody-based vector has been generated they can be tagged with radionuclides (PET, SPECT), magnetic nanoparticles (MRI) or fluorescence/bioluminescence (optical) probes that enable a variety of imaging modalities. Although PET is more sensitive than SPECT, the latter offer advantages such as broad availability and lower costs of radioisotopes and γ -scanning instruments. In addition, since SPECT radionuclides emit photons with different energies, several biomarkers can potentially be distinguished at the same time, as opposed to PET radionuclides which all emit the same energy photons (511 keV). MRI is a powerful imaging modality with regards to high spatial resolution (≤ 100 microns) and tomographic capabilities, but the low signal sensitivity has been a major limitation for molecular imaging. However, the recent development and the increased sensitivity of magnetism-engineered iron oxide (MEIO) nanoprobe obtained when conjugated to Herceptin may make antibody fragments attractive MRI imaging agents ¹⁷. The extremely high sensitivity of optical imaging approaches ($10^{-15} - 10^{-17}$ mol/L for bioluminescence; $10^{-9} - 10^{-12}$ mol/L for fluorescence ¹⁸) for real-time imaging of small animal models provide low cost alternatives to nuclear medicine imaging approaches. The major disadvantage of optical imaging using visible light is poor tissue penetration (<1 cm) due to scatter and absorption of light. Bioluminescence has some advantages over fluorescence, since signal is produced in the presence of substrate (no excitation light source is needed) and there is no background autofluorescence. However, for optical imaging, tomographic imaging remains a challenge. This review focuses on the use of engineered antibody fragments as probes or vectors for non-invasive imaging of tumors, with an emphasis on nuclear medicine applications.

RECOMBINANT ANTIBODY FRAGMENTS FOR IMAGING

1. Monovalent single-chain Fv fragments

The scFv fragment consists of variable light (V_L) and heavy (V_H) domains joined by a flexible peptide linker that can be 12–25 residues long (Figure 1). The resulting protein being 1/6 of the size of an intact antibody (150 kDa) retains the specificity and affinity of the parental antibody. Although the V domains can be in either orientation i.e. V_L -linker- V_H or V_H -linker- V_L , the orientation can affect expression ^{19, 20}, stability and antigen binding activity ²¹. Early biodistribution and imaging studies in planar gamma cameras revealed that although scFv molecules cleared very rapidly from blood, they were able to localize efficiently to their target ^{22–27}. However, issues with direct iodination such as loss of immunoreactivity and deiodination reduce the signal in the target tissue. For this reason scFv molecules have been radiolabeled with radiometals and other radionuclides. Several groups have used technetium-99m for two reasons: 1) its short physical half-life (6 h) is compatible with the short biological half-life of scFv, and 2) carrier-free ^{99m}Tc is generator produced and readily available in hospital nuclear medicine departments. Genetic engineering approaches for site-specific ^{99m}Tc-labeling have been created by C-terminal addition of a cystinyl peptide (G)₄C ²⁸ or a cys-his₆ peptide ²⁹ for chelation chemistry, metallothionein-myc peptide for direct radiolabeling ²⁷ and his₆ tag for using Tc(I)-carbonyl complex ³⁰. Radiometal labeling of scFv

with ^{177}Lu and ^{111}In following conjugation to DOTA or DTPA, respectively 31, 32 resulted in elevated kidney retention and only a few %ID/g in the tumor in xenograft-bearing mice. When a disulfide stabilized anti-Tac scFv (dsFv) radiolabeled with ^{18}F was evaluated in ATAC4 tumor bearing mice, maximum retention in the tumor was 4.2% ID/g at 45 min p.i. and maximum retention in the kidneys was 303% ID/g at 15 min p.i. 33. Thus, kidneys are the dose-limiting organ of this fragment. Fluorescence imaging using fluorescent-conjugated scFv molecules for non-radioactive immunodetection of tumors has also been investigated 34, 35. Using cyanine fluorochromes Cy7 (infrared) and Cy5.5.18 (far infrared) rapid secretion via the renal route was observed early whereas strong accumulation of fluorescence in tumor was evident at 24 h p.i.

The major limitations of scFv molecules are low functional affinity and short *in vivo* half-life (Figure 2) due to their valency and small size, respectively. Consequently, rapid dissociation from the target antigen due to monovalent binding will result in modest retention time in the target and potentially poor image quality 36. Still they remain attractive candidates as they can easily and cost effectively be expressed in bacteria. To extend the *in vivo* half-life, scFv molecules have been conjugated to polyethylene glycol (PEG) polymers and human serum albumin (HSA). Following site-specific PEGylation of 5, 20 and 40 kDa maleimide-PEG polymers to a scFv, prolonged biological half-lives *in vivo* correlating to the molecular mass of the polymer was observed 37. HSA has a serum half-life of 19 days and Yazaki *et al* 38 fused HSA to anti-CEA T84.66 scFv molecule and evaluated the fusion molecule by both SPECT and PET using different radionuclides. SPECT images with ^{125}I and ^{111}In -DOTA-labeled scFv-HSA demonstrated rapid clearance and excellent tumor uptake. PET imaging was carried out with one tumor bearing mouse injected with ^{64}Cu -DOTA-scFv-HSA. In this animal, tumor localization was evident at 4 h which reached highest intensity at 24 h p.i. The anti-CEA scFv-HSA fusion protein primary clearance route was through the liver (MW = 90 kDa). It exhibited significant slower blood clearance and a higher tumor uptake than the minibody 39. These results are encouraging and be utilized as an alternative way to overcome the very rapid clearance of scFv fragments.

2. Di- and multivalent single-chain Fv fragments

The monovalency of scFv is a significant limitation to tumor retention and numerous approaches to genetically engineer monovalent scFv into multivalent fragments with greater avidity have been pursued. Joining two anti-TAG-72 CC49 scFv molecules in tandem to produce divalent sc(Fv)₂ have resulted in spontaneous dimerization to a tetravalent [sc(Fv)₂]₂ with affinity and tumor retention similar to the intact parental antibody, but with a more rapid blood clearance 40. *In vivo* studies with $^{99\text{m}}\text{Tc}$ -CC49 sc(Fv)₂ and [sc(Fv)₂]₂ demonstrated longer blood clearance and higher tumor retention with the tetravalent [sc(Fv)₂]₂ 41. Chemical cross-linking of anti-TAG B72.3 scFv molecules using bis-maleimide cross-linkers have been employed to produce dimers or trimers 42. Both exhibited rapid clearance and similar tumor uptakes (~10% ID/g at 24 h p.i) *in vivo*, but high kidney retention was observed only with the radiometal labeled dimer. In another study, SPECT imaging of tumor bearing mice injected with a covalent linked ^{125}I -sc(Fv)₂ (divalent) against placental alkaline phosphatase (PLAP), showed improved tumor uptake and longer retention time in the tumor compared to the monomeric scFv 43. Similarly, improved tumor uptake over the 741F8 scFv monomer was achieved when it was made into a dimer, bridged via a C-terminal gly₄cys₂ peptide 44.

Use of multimerization domains or sequences to produce high avidity scFv molecules has also been explored. Streptavidin-scFv fusion for production of tetravalent and bifunctional scFv molecules 45, 46 has largely been exploited for *in vivo* pretargeting approaches for delivery of therapeutics conjugated to biotin 47–51. However, streptavidin-based pretargeting approaches have two potential limitations: renal toxicity 50 and highly immunogenic streptavidin 52. PET

imaging using ^{68}Ga -DOTA-biotin-streptavidin revealed high blood-pool and renal activities at 90 min p.i.⁵⁰. SPECT images of ^{67}Ga -DOTA-biotin after pretargeting with succinylated anti-TAG-72 CC49 scFv-streptavidin showed targeting to the tumor (3.8% ID/g at 24 h). Biodistribution data showed that activities in blood and organs were below 1% ID/g and that there was 30% reduction of kidney uptake relatively to the control. Recently two research groups have used collagen derived sequences to produce scFv-trimers^{53, 54}. Fluorescent imaging was carried out with anti-CEA MFE-23 and anti-laminin L36 scFv molecules fused to the N-terminal collagen XVIII NC1 subdomain that forms non-covalent bound trimers of collagen alpha chains⁵⁴. The so-called “trimerbodies” were labeled with the near-infrared fluorochrome cyanine-5 (Cy5) and administered to tumor bearing mice. Strong signal was observed in the tumors as early as 3 h p.i. that persisted to 48 h, whereas mice injected with control trimerbody showed no signal in the tumors. Monomeric scFv showed localization to tumor at 3 h only, but at a much lower level. Another domain that has been used for multimerization of scFv is the p53 tetramerization domain^{55–58}. Various versions of leucine zippers or four-helix bundles have been fused to scFv C-terminus via IgG3 hinge region for production of dimers^{59, 60}. *In vivo* studies with these dimers, demonstrated intermediate blood clearance activity relatively to the monomer and the intact antibody⁶⁰. In a later study, tumor targeting of mono-, di-, and tetrameric variants of anti-Her2 4D5 scFv was compared⁵⁸. C-terminal helix-turn-helix domain and human p53 protein was used to make dimers and tetramers, respectively. *In vivo*, the $^{99\text{m}}\text{Tc}$ -labeled tetramer demonstrated the longest serum persistence and highest tumor accumulation (4.3% ID/g at 24 h p.i.). Other multimerization domains that have been used are C4 binding protein to produce scFv octamers⁶¹, and recently dimeric and tetrameric scFv molecules fused to uteroglobin was described⁶². However, these have not been evaluated *in vivo*. The above *in vivo* studies provide compelling evidence that the avidity effect is important for tumor retention. In addition, since blood clearance is inversely related to the size, the larger sized antibody fragments all demonstrate slower clearance and longer exposure to the target, thus improving tumor targeting and retention.

Conjugation of scFv to nanoparticles has also been described^{63–65}. One study used anti-Her2 quantum dot-conjugated immunoliposomes-based nanoparticles (QD-ILs) for optical imaging of xenografts⁶⁴. These nanoparticles consisted of a liposomal core with incorporated PEG-linked anti-HER2 scFv and QDs. *In vivo* studies revealed that the QD-ILs exhibited intermediate clearance ($T_{1/2} = \sim 2.9$ h) relatively to free QDs ($T_{1/2} < 10$ min) and free liposomes ($T_{1/2} = \sim 7.7$ h). However, optical imaging showed that both targeted and non-targeted nanoparticles exhibited equal tumor accumulation ($\sim 14\%$ of total body fluorescence) at 24 hours p.i. The authors explained this was consistent with the enhanced permeability and retention effect previously observed with long circulating liposomes. Thus, antibody mediated *in vivo* targeting was not observed in this study. In another study, anti-MUC-1 scFv fragments were conjugated to superparamagnetic iron oxide (SPIO) nanoparticles⁶³. At 24 hours after injection, 5% ID/g was in the tumor as shown by whole-body autoradiography. In a recent study, an anti-epidermal growth factor receptor (EGFR) scFv was conjugated to surface functionalized QDs and magnetic iron oxide (IO) nanoparticles⁶⁵. *In vivo* targeting of both nanoparticles following systemic delivery was demonstrated in an orthotopic pancreatic cancer model. Frozen tissue sections of mice injected with anti-EGFR-scFv-QD were examined by fluorescence microscopy, whereas mice injected with anti-EGFR-scFv-IO were evaluated by MRI imaging. Higher tumor uptake than background activity was observed with both nanoparticles. However, uptakes were also observed in the liver and spleen, although lower than those seen with the non-targeting nanoparticles.

3. Diabody (scFv dimer)

The easiest approach to engineer scFv dimers and higher orders of multimers is shortening the linker to <10 residues between the variable domains. The shorter linker opens up the scFv and

forces it to cross-pair with another scFv molecule to form a non-covalent bound dimer that is called diabody (Figure 1) ⁶⁶. By reducing the linker length further (≤ 3 aa) non-covalently bound scFv trimers and tetramers can be produced ⁶⁷. However, the pattern of oligomerization is not straight forward as it is influenced by the variable domain sequence and their orientation in the scFv fragment ⁶⁸. The stability of trimers and tetramers is an issue as demonstrated *in vivo* with an ¹¹¹In-labeled anti-Lewis Y trimeric/tetrameric “multimer” ⁶⁹. Although tumor retention at 6 hours p.i. was similar to that with the F(ab')₂ at 24 hours p.i, high renal accumulation was observed which was probably due dissociation into monomers. The authors conclude that instability will prevent development of these fragments into imaging agents.

Diabodies on the other hand form stable non-covalent dimers that have been shown to have a slightly longer blood clearance than scFv molecules (Figure 2). The larger size (50 kDa) and divalency have been attributed to their improved tumor uptake ⁷⁰. Early SPECT imaging studies with that ¹²³I-labeled anti-CEA T84.66 diabody demonstrated that tumors could be readily imaged at 6 h p.i ⁷¹. This fragment reached a maximum tumor uptake at 2 h of 13.68 (1.49)% ID with a tumor to blood ratio of 2.9. At 6 h the activity in the tumor was 9.23(0.44)% ID/g and the tumor to blood ratio was 9.4. The uptake in the tumor at 24 h was similar to that of another anti-CEA, CB/ior-CEA.1, diabody (5 aa linker) that showed accumulation of 3.1% ID/g at 24 hours ⁷². The anti-CEA T84.66 diabody has been radiolabeled with several different positron emitting radionuclides (¹⁸F, ⁶⁴Cu, ¹²⁴I) and evaluated in tumor-bearing mice by small animal PET (Figure 3A). ¹²⁴I-labeled diabody exhibited excellent, high contrast images with target to background ratios of 3.95 at 4 h and 10.93 at 18 h ⁷³. Less contrast was achieved with ⁶⁴Cu-DOTA diabody (Figure 3A). The anti-CEA diabody was also radiolabeled with ¹⁸F using N-succinimidyl-4-¹⁸F-fluorobenzoate (¹⁸F-SFB) and evaluated by PET imaging in xenografted mice ⁷⁴. Clear delineation of the positive tumor was obtained as early as 1 hour after injection of the ¹⁸F-FB-T84.66 diabody with clearance predominantly via the kidneys. This study suggests that the diabody is compatible with a short lived radionuclide for same day imaging.

Enzymes that can catalyze a light-producing reaction (a process called bioluminescence) are known as luciferases. The light is produced following injection of a substrate for the enzyme. Luciferases are mainly used as reporter genes with firefly luciferase being the most commonly used for imaging ⁷⁵. Other luciferases such as renilla luciferase (RLuc) and gaussia luciferase (GLuc) from the sea pansy *Renilla reniformis* marine copepod *Gaussia princeps*, respectively, have been fused to the anti-CEA diabody and evaluated by optical bioluminescence imaging (Figure 3B) ^{76, 77}. Signal in the tumor was observed from 2 to 24 h with the diabody-RLuc8 variant with the highest intensity at 4 to 8 hours p.i. ⁷⁷. The tumors in mice injected with diabody-GLuc Δ 15, also exhibited highest intensity at 4 hours p.i ⁷⁶. However, although the diabody-GLuc Δ 15 was brighter than diabody-RLuc8 *in vitro*, the overall *in vivo* performance of diabody-GLuc Δ 15 was poorer than that of the diabody-RLuc8 with regards to stability, tumor uptake and sustained targeting out to 24 hours p.i. Still, these studies show that diabodies can be used as targeted vehicles to carry functional units for optical imaging of cell surface targets.

Diabodies to several other targets have also been evaluated *in vivo*. The human anti-Her2 C6.5 diabody is another well-characterized antibody fragment that has demonstrated significant tumor uptakes (~6.5 %ID/g and a tumor-to-blood ratio of about 9 at 24 hours p.i.) in xenograft-bearing animals ^{70, 78}. This diabody was radiolabeled with ¹²⁴I using both direct and indirect labeling methods ^{79, 80}. PET images of mice bearing Her2-positive xenografts following injection of directly radioiodinated diabody, showed excellent localization to tumors as well as significant uptake in the thyroid and stomach which are the natural sites of iodine metabolism. Indirectly labeled diabody with the water-soluble form of Bolton-Hunter reagent, SHPP, on lysine residues attenuated the uptake of free, metabolized radioiodine in thyroid and

stomach but did not enhance the uptake in the tumors⁸⁰. Animals injected with SHPP-labeled diabody had a higher retention of radioactivity in non-targeted tissues than animals injected with directly labeled diabody, resulting in a higher background signal in the images. However, tumors were clearly delineated at 48 hours p.i. More recently, a humanized anti-PSCA diabody was evaluated by PET imaging in mice bearing prostate xenografts following radioiodination with ¹²⁴I⁸¹. In this study, activity in the tumor was observed at 4 hours with most of the activity gone at 20 hours p.i., but the highest tumor-to-background-ratio was obtained at 12 hours p.i. Better tumor accumulation in human prostate xenografts was recently achieved with ⁸⁶Y-CHX-A''-DTPA-antimindin/RG-1 19G9 diabody⁸². At 48 h post injection, significant accumulation of activity was seen in the tumors by PET, whereas no activity in the tumor was detected with the scFv monomer. Diabodies against PSCA and Her2 have also been radiolabeled with ¹⁸F-SFB and evaluated by PET in xenograft bearing mice^{83, 84}. Localization to tumors and high contrast images were obtained by 4 to 6 hours p.i. suggesting that the half lives of the nuclide and the antibody fragment were compatible for early imaging.

One issue with radiolabeling smaller antibody fragments is that reactive residues may be present in critical regions of the antibody. For this reason approaches for site specific modification have been developed. The anti-ED-B domain of fibronectin L19 diabody and two variants with different ^{99m}Tc binding motifs (i.e. Gly₃CysAla or His₆ peptide for direct site-specific radiolabeling) C-terminally were evaluated in murine F9 teratocarcinoma tumor-bearing mice⁸⁵. Although the *in vitro* binding to ED-B fibronectin was the same, their biodistribution differed. All three showed similar tumor uptakes of 7.7–9.4% ID/g at 3 hours that was reduced to 2.8–5.7% ID/g at 24 hours p.i. The L19 Db that was randomly chemically modified by a MAG2-type chelator and indirectly radiolabeled demonstrated slower blood clearance than the L19 Db-Gly₃CysAla which resulted in a higher background activity in the scintigraphic images. The L19 Db-His₆ showed elevated accumulation of radioactivity in the kidneys (145% ID/g at 3 hours) in comparison to the other two Db variants (8.6 and 15.2% ID/g at 3 hours). At 24 hours the activity of L19 Db-His₆ in the kidney was reduced to 72.4% ID/g versus 2.6 and 3.0% ID/g of the other two diabodies. The authors conclude that L19 Db-Gly₃CysAla showed the most favorable biodistribution and imaging properties which could potentially be useful to image angiogenesis-associated ED-B fibronectin-expressing tumors.

Another approach has been to add a C-terminal cysteine, preceded by two glycines, to diabodies for thiol-chemistry⁸⁶. Cys-diabodies against CEA, Her2, CD20 and PSCA have been generated and shown that this fragment will exist exclusively as disulfide-bonded dimer that can be reduced and chemically modified using a thiol-specific bifunctional chelating agent, for attaching radionuclides⁸⁶, fluorophores⁸⁷ and for targeting nanoscale particles such as quantum dots (Qdots)⁸⁸. The anti-CEA cys-diabody was evaluated *in vivo* following site specific radiolabeling with ⁶⁴Cu to a macrocyclic chelate DOTA peptide–hexanevinyl sulfone (DOTA-GLGK-HVS) conjugated to the C-terminal cysteine⁸⁶. The ⁶⁴Cu-DOTA-GLGK-HVS Cys-diabody behaved similarly to its parental diabody with specific targeting to tumors observed by PET imaging at 4 and 18 h post-injection. More recently an anti-CD20 cys-diabody was compared with its parental diabody by PET imaging following random radiolabeling with ¹²⁴I⁸⁹. Again, very similar biodistribution was observed for the two fragments suggesting that the tethering of the C-termini of the diabody subunits did not affect the *in vivo* tumor targeting and blood clearance properties. Thus, this format appears to be a general platform for site-specific conjugation of antibody fragments with functional payloads.

4. Minibody (scFv-C_H3 dimer)

To overcome the accumulation in the kidneys seen with the diabodies, larger fragments that exceeded the renal clearance threshold (<60 kDa) have been designed (Figure 1). For example, human immunoglobulin constant domains have been used to produce intermediate-

sized antibody fragments with longer serum-half-lives (6–11 hours) (Figure 2). The first scFv molecule that was joined to human IgG1 C_H3 domain was derived from the anti-CEA T84.66 mAb and was referred to as a minibody⁹⁰. The fusion was either by a two amino acid spacer (LD minibody) that formed non-covalent dimer or via the human IgG1 hinge and a flexible linker peptide (FLEX minibody) that formed covalent dimers⁹⁰. The ¹²³I-FLEX minibody exhibited superior tumor targeting (32.9% ID/g) at 6 hours after injection, relatively to that of the ¹²³I-LD minibody (16.4% ID/g) which had substantially faster blood clearance kinetics. At 6 hours, the tumor-to-blood ratio of FLEX-minibody was only 2 which increased to 64.9 at 48 hours p.i. Initial SPECT images with the anti-CEA ¹²³I-minibody showed localization to the tumors at 4 hours, and that the background was almost completely cleared at 19 hours allowing distinct delineation of the tumors. As a result of these initial studies, the FLEX minibody format was used in all subsequent studies.

ImmunoPET with the anti-CEA minibody is shown in Figure 3. This minibody demonstrated its suitability as an imaging agent with rapid high-level accumulation of activity in xenografts and rapid disappearance from the circulation^{73, 91}. Serial small animal PET imaging with ⁶⁴Cu-DOTA-minibody demonstrated rapid and specific localization to the positive tumor with increasing accumulation of activity over time (from 2 to 24 hours p.i.) that was >20% ID/g at 24 hours with a tumor-to-soft-tissue ratio of 6⁹¹. As expected, high persistent activity in the liver was also seen with activity moving into the GI-tract at the late time-point. PET images with ¹²⁴I-minibody produced excellent images at 18 hours p.i. with tumor uptakes of 21% ID/g and tumor-to-background ratio of 26.2⁷³. The high ratio is due to the rapid clearance from the blood combined with fast metabolism and clearance of radioiodine from non-targeted tissues. In comparison to FDG scan, both radiometal labeled and radioiodinated minibody produced a much cleaner and higher contrast image.

Minibodies have also been produced against Her2 and prostate stem cell antigen (PSCA) expressed in breast and prostate cancers^{92–94}. Although both anti-Her2 and anti PSCA minibodies demonstrated similar pharmacokinetics to the anti-CEA minibody and localized specifically to tumors, they accumulation in tumors was considerable lower. Activity in the tumor was about 5% ID/g at 12 to 24 h with anti-Her2 ¹³¹I-10H8 minibody with tumor-to-blood ratios of 1.1 at 12 h that increased to 3 at 48 hours⁹⁴. This lower activity was explained by internalization of the minibody upon binding, followed by metabolism and rapid excretion of radiolabel from the cells. Biodistribution with anti-Her2 ¹¹¹In-DOTA-10H8 minibody demonstrated that the radioactivity remained in the tumor, increasing the tumor-to-blood ratio to 13.3 at 48 hours p.i.⁹³. Unexpectedly, the kidneys contained higher activity than the liver which was attributed to the presence of a cross-reactive antigen. A different minibody derived from Herceptin (Herc. Mb) was evaluated by PET (Figure 4)⁹³. Although PET imaging with anti-Her2 ⁶⁴Cu-DOTA-4D5v8 minibody showed targeting to positive tumor, only about 4% ID/g was in the tumor from 4 to 48 hours p.i. Since the activities in the liver and kidneys were 3 to 4-fold higher, high background and less contrast were achieved with this fragment. When this fragment was radioiodinated with ¹²⁴I, less activity was seen in the tumor, whereas clear delineation of the tumor was achieved with the anti-Her2 ¹²⁴I-C6.5 minibody (Figure 4). This difference is probably due to different affinities of the fragments and that C6.5 internalization rate varies in different cell lines⁹⁵. Biodistribution with the anti-PSCA ¹³¹I-2B3 minibody resulted in accumulation of 9% ID/g in the tumor, and the tumor-blood-ratio was 2.8 at 21 hour p.i.⁹². Figure 4 shows PET imaging with the anti-PSCA ¹²⁴I-2B3 minibody. Specific localization to PSCA expressing LAPC-9 xenografts, with uptake of 5.2% ID/g and tumor-to-blood ratio of 1.1 at 21 hours was achieved⁹². This was close to the uptake (6.6% ID/g) obtained with the intact parental antibody at 168 hours p.i.⁹⁶. Thus, in this tumor model early, good contrast images of PSCA expressing xenografts were obtained with the minibody. Recently, a minibody against CD20 antigen expressed on B-cell lymphoma was generated from rituximab (Rituxan, Genentech)⁹⁷. This fragment differed from the above minibodies in that

the 218 linker 98 was used between the variable domains, and the scFv was fused to the complete human IgG4 hinge and C_H3 domain. PET images with anti-CD20 ⁶⁴Cu- and ¹²⁴I-rituximab minibody (Rx. Mb) are shown in Figure 4. The ¹²⁴I-rituximab minibody showed excellent targeting (12.9% ID/g) to tumor with very little activity in negative tumor and other tissues and a tumor to blood ratio of 7.5 at 21 hours, whereas less contrast was obtained with the ⁶⁴Cu-DOTA-Rx. Mb ⁹⁷. These studies show that although the pharmacokinetics is similar for this antibody fragment format in the different animal models, tumor uptake varies depending on factors such as antigen expression, whether the target internalizes or not upon antibody binding, radiolabel and specificity/affinity.

Another similar sized antibody fragment referred to as “small immunoproteins” (SIP) consisting of scFv joined to the C_H4 domain of the secretory isoform S2 of human IgE for dimerization and further stabilized by a C-terminal disulfide bond has been generated ⁹⁹. Tumor targeting of anti-ED-B domain of fibronectin L19-SIP was 2–5 times higher than that of (scFv)₂, reaching a maximum uptake at 4–6 hours p.i. Accumulation of radioactivity in the mouse embryonal teratocarcinoma F9 tumor model was 3–4 times higher (12–18% ID/g) than in SKMEL-28 tumor model due to their difference in angiogenic activity. Although PET imaging of ⁷⁶Br-L19-SIP showed accumulation in F9 tumors from 5 to 48 h, persistent activity in the blood and stomach due to debromination resulted a tumor to background ratio of <2 at 48 hours p.i ¹⁰⁰. Recently, this fragment was radiolabeled with ¹²⁴I and evaluated in mice bearing human head and neck squamous cell carcinoma (HNSCC) FaDu xenografts ¹⁰¹. In this model, tumor accumulation reached a maximum of approximately 11% ID/g at 6 hours p.i., and at 48 hours the tumor uptake was about 5% ID/g and the tumor to blood ratio was 13.5 which increased to 45.9 at 72 hours. This was in concordance with ¹³¹I-labeled L19-SIP biodistribution, thus authors conclude that imaging with iodine-124 can be used to predict ¹³¹I-L19-SIP biodistribution. Another SIP has been made from affinity matured human anti-tenascin-C G11 mAb ¹⁰². However, only 0.85% of ID/g of ¹²⁵I-G11-SIP accumulated in U87 human glioblastoma xenografts at 24 hours p.i. which was similar to the tumor uptake (0.71% ID/g) of ¹²⁵I-labeled G11 scFv alone at 24 hours. The authors do not address this low uptake and one can only speculate that such low uptake was due to instability of the protein, low antigen expression in target and/or internalization of the G11-SIP with rapid dehalogenation and secretion of the label in this tumor model.

Recently, a so-called “miniantibody” against mindin/RG-1 composed of IgE-C_H4 dimerization domain and IgG1 hinge and modified first β-strand peptide residues of IgG1 C_H2 was evaluated by PET following conjugation of CHX-A”-DTPA and radiolabeling with ⁸⁶Y ⁸². At 24 hours p.i. about 4% ID/g was in the blood and about 13% ID/g was localized to LNCaP (prostate cancer) xenografts. At 72 hours p.i. the tumors were still visible and the background activity was greatly reduced. When the same fragment was labeled with ¹¹¹In, biodistribution studies revealed that the activities in the tumors and blood at 48 hours were approximately 14% ID/g and 1% ID/g, respectively. This resulted in a tumor to blood ratio that was better than that of the intact antibody (2.2 to 1), but worse than that of the diabody (80 to 1) at 48 hours p.i. Thus, the authors conclude that the diabody may be more suitable for radiodiagnostic applications.

5. scFv-Fc (scFv-C_H2-C_H3 dimers)

Larger antibody fragments that include the entire Fc region (Figure 1) have also been evaluated by small animal PET imaging (Figure 5). However, the neonatal Fc receptor (FcRn) which binds to the IgG Fc region is responsible for the prolonged serum half-life of intact antibodies and imaging with intact antibodies requires days to clear from the blood in order to produce high contrast images. However, clearance can be tailored by modifying the FcRn interaction in the Fc region. This was elegantly shown in a study with anti-CEA T84.66 scFv-Fc fragments ¹⁰³. Site-specific mutations of the IgG1 Fc residues involved in this interaction resulted in five

variants (I253A, H310A, H435Q, H435R, and H310A/H435Q) that each exhibited distinct blood clearances in mice that ranged from 83.4 to 7.96 hours, which was much faster than that of the wild-type (~12 days). SPR analyses using human FcRn, also demonstrated binding of scFv-Fc WT whereas no interaction was obtained with the scFv-Fc H310A/H435Q fragment¹⁰⁴. These fragments were also radioiodinated with ¹²⁴I and evaluated by PET in xenografted mice. Although the wild-type had the highest tumor uptake (42.5% ID/g at 48 h p.i.) it also had the lowest contrast relatively to the intermediate clearing (I253A and H310A) and the fast clearing (H310A/H435Q) scFv-Fc fragments. The blood clearance of the scFv-Fc DM shown in Figure 2A, demonstrates that this fragment persists longer in the circulation than the minibody fragment that results in high tumor uptake (Figure 2B). The PET images of ¹²⁴I- and ⁶⁴Cu-DOTA- scFv-Fc H310A/H435Q also referred to as scFv-Fc double mutant (scFv-Fc DM) show high, specific tumor uptakes in xenografts (Figure 5A). The pharmacokinetics of radioiodinated versus radiometal-labeled I253A, H310A and H310A/H435Q scFv-Fc variants were further evaluated in xenografted mice in order to predict their therapeutic potential¹⁰⁵. Tumor uptakes were inversely related to blood clearance and hepatic radiometal activity correlated with the blood clearance rate of the fragment i.e. faster clearance resulted in higher activity. Based on the biodistribution data with ¹²⁵I and ¹¹¹In, it was predicted that the fast clearing scFv-Fc DM would be able to deliver >7,000 cGy to the tumor with favorable tumor to liver and kidney ratios when radiolabeled with ¹³¹I, whereas as for ⁹⁰Y therapy a slow clearing antibody would be the protein of choice as the liver/kidney activities would be lower.

The scFv-Fc DM fragment has also been evaluated in other tumor models. An anti-Her2 scFv-Fc DM fragment was evaluated by PET in xenografted mice following conjugation with DOTA and radiolabeling with ⁶⁴Cu⁹³. The scFv-Fc DM fragment exhibited over 2-fold improved tumor targeting and reduced kidney activity relatively to the anti-Her2 minibody fragment which was probably due to its slightly longer residence time in the blood. When this fragment was labeled with ¹²⁴I, very low activity was observed in the tumor. In another recent study, an anti-CD20 scFv-Fc DM fragment with IgG4 Fc was evaluated in tumor bearing mice following radioiodination with ¹²⁴I (Figure 5B)⁹⁷. Although rapid tumor localization was observed, the activities in the tumor and the blood were 2-fold lower than of the minibody. Such difference was not observed with the anti-CEA (Figure 2A) and anti-Her2 fragments. Thus it appears to be related to the change of IgG Fc isotype. Intact human IgG4 has been reported to clear faster than human IgG1 in both humans and mice^{106, 107}. Consistent with this, a lower background activity of the radioiodinated anti-CD20 scFv-Fc DM fragment than that of the anti-CEA scFv-Fc DM at 18–20 hours p.i. was observed. Thus, the introduced mutations in IgG4 Fc may accelerate the scfv-Fc fragment to clear faster than the minibody. Figure 5B also shows the images obtained with ⁶⁴Cu-DOTA scFv-Fc DM fragment.

A rapid method to generate scFv-Fc fragments targeting endothelial cell from binders isolated from phage display libraries and *in vivo* evaluation by SPECT have been described¹⁰⁸. Using this approach, three antibodies were identified that, when converted to scFv-Fc using mouse IgG1 Fc, targeted the lungs in rats with uptakes of 30–40% ID/g at 1 and 2 hour p.i. Since the blood activities were less than 2% ID/g, high contrast images were achieved early.

IMPACT OF ANTIBODY MODIFICATIONS ON IMAGING

From the numerous studies performed with the different engineered antibody fragments there are several factors such as the molecular weight, Fc domains, valency and specificity that will influence targeting and pharmacokinetics. Larger fragments above 60 kDa will clear via the liver, whereas those below this size will clear via the kidneys. Presence of Fc domains will increase the serum residence time, and increase the exposure time to the target. However, for imaging purposes a more rapid clearance from the blood is warranted in order to increase

contrast and sensitivity. Difficulties in localizing and accumulating activity in target tissue are related to specificity and avidity (i.e. number of antigen binding sites). In addition, the number of target antigen per cell and whether it internalizes or not will affect accumulation in target tissue. Antibody mediated internalizing of targets followed by catabolism via lysosomal targeting and proteolytic degradation will reduce tissue uptake. The rate of antigen internalization varies among different antigens. For example CEA internalizes slowly at a rate of approximately $0.001 \text{ minutes}^{-1}$ ¹⁰⁹, whereas Her2 has up to 100 times faster internalization rate when associated with EGFR¹¹⁰. This may explain the lower accumulation of activity in Her2 tumors observed with ^{124}I -labeled Herceptin minibody and scFv-Fc DM in Figures 4 and 5B. In contrast, tumor was clearly delineated with ^{124}I -labeled C6.5 minibody (Fig. 5B). The C6.5 diabody has been reported to differ in internalization rate in different cell lines [i.e. relatively slowly by SK-OV-3 cells (10% in 3 hours) and rapidly by MDA-361/DYT2 cells]⁹⁵. Thus, it is possible that the C6.5 minibody internalizes more slowly than the Herceptin minibody in this tumor model. Since it appears that the mAb and scFv internalization rates are determined by antigen recycling, rather than antigen endocytosis^{111, 112}, antibodies with greater dissociation rates than antigen internalization rates can minimize catabolism.

The presence of shed antigen in the blood will deplete the pool of free antibodies available to reach the target. Once bound, the abnormal physiology in solid tumors limits inward diffusion and extravasation across capillary walls into the surrounding tissue by the antibody due to presence of a high interstitial fluid pressure gradient. Although smaller antibody fragments can penetrate tumors better than larger fragments, the affinity of the scFv fragments has also shown to affect tumor uptake i.e. as affinity increases, penetration decreases which is referred to as the “binding-site barrier”^{113–115}. Anti-Her2 scFv with different affinities demonstrated that a minimum binding affinity of 10^{-8} to 10^{-9} M was required for retention in tumors, as a scFv with 10^{-7} M affinity failed to accumulate more than the negative control scFv¹¹⁶. Increasing the affinity to 10^{-10} to 10^{-11} failed to increase the tumor accumulation^{114, 117}. Thus, the higher tumor accumulation of C6.5 minibody in Figure 5B may be due to the higher affinity of C6.5 IgG (5.4×10^{-11} M¹¹⁸) versus that of Herceptin (5×10^{-9} M).

Other factors that may affect the targeting are the nature of label used and the labeling chemistry employed. Several positron emitters for immunoPET are currently under investigation. These can be grouped according to their physical half-lives ($t_{1/2}$) that ideally should be paired with the biological half-lives of the antibody fragments. Short-lived positron emitters are ^{68}Ga ($t_{1/2} = 1.13$ h) and ^{18}F ($t_{1/2} = 1.83$ h) which are suitable for rapid clearing fragments such as scFv and diabodies. Intermediate-lived positron emitters are ^{64}Cu ($t_{1/2} = 12.7$ h), ^{86}Y ($t_{1/2} = 14.7$ h) and ^{76}Br ($t_{1/2} = 16.2$ h) which are suitable for antibody fragments with intermediate clearance properties such as minibodies and modified scFv-Fc fragments. Long-lived positron emitters are ^{89}Zr ($t_{1/2} = 78.4$ h) and ^{124}I ($t_{1/2} = 100.3$ h) which are suitable for intact antibodies and scFv-Fc WT. Since long lasting radionuclides have been successfully used with rapid clearing antibody fragments and produced excellent, high contrast images^{73, 97}, it does not seem to be crucial to pair the physical and biological half-lives of the radionuclide and antibody, respectively. One may consider the target and use bifunctional chelates for stable, indirect radiolabeling chemistry when targeting rapid internalizing targets, as the label will be trapped in the lysosomes leading to increased accumulation of activity over time. Since directly iodinated proteins will be rapidly catabolized with the radioactivity excreted and eliminated via the kidneys, only targets with slow internalization rates are suitable to be imaged with this label. However, there are exceptions as demonstrated with C6.5 Mb in Figure 4. Another issue is that critical residues may be modified and impair the function of the antibody, especially as the fragment become smaller. If this is the case, site-specific conjugation and radiolabeling chemistry can be employed in order to retain function.

OTHER PROMISING NEW DIRECTIONS

Over the past 10–15 years, the antibody engineering field has moved towards even smaller scaffolds, encompassing a range of protein domain-based frameworks that are neither conventional antibodies nor peptides. These are characterized by small molecular size (single polypeptide chain format), high stability (thermodynamic and chemical), high solubility, and architecture suitable for modifications. Other attractive features may include high bacterial expression for inexpensive production, absence of disulfide bonds and human origin. These protein based reagents represent a new generation of highly specific and sensitive binding molecules that are immunoglobulin or non-immunoglobulin based [119–120]. Immunoglobulin based scaffolds include immunoglobulin variable fragments (Fv), single domain antibodies from camelids and sharks, T cell receptor (TCR), cell adhesion molecules and fibronectin domains. Among non-immunoglobulin based scaffolds are affibodies, ankyrins, adnectins, avimers and anticalins.

Nanobodies® are derived from naturally occurring antibodies that lack the light chain. An anti-EGFR llama single-domain antibody fragment (8B6 Nanobody; 12 kDa) was recently evaluated for *in vivo* radioimmunodetection [121]. The 8B6 Nanobody was radiolabeled with ^{99m}Tc via its C-terminal histidine tag and evaluated in mice bearing high (A431) or moderate (DU145) EGFR expressing xenografts by SPECT. Although rapid clearance ($t_{1/2\beta} = 1.5$ h) from the blood was observed, a significantly higher radioactive uptake was seen in the high EGFR expressing A431 xenografts, demonstrating specificity at 3 hours post injection. Another camelid Nanobody targeting CEA was also radiolabeled with ^{99m}Tc on a hexahistidine tag and evaluated for tumor targeting by SPECT [122]. At 3 hours p.i. 3.2% ID/g was in the positive tumor, which was 3 and 6 times higher than the activities in the negative tumor and blood, respectively. Images showed specific localization to the positive tumor, and background activities in the liver and kidneys.

Affibodies (7 kDa), derived from staphylococcal surface Protein A, are one of the most characterized non-immunoglobulin based scaffolds (reviewed in [123]). Affibodies to Her2 have been radiolabeled with ¹²⁵I, ¹¹¹In, ^{99m}Tc, for SPECT imaging and ¹⁸F for PET imaging. Clear, high contrast images of the tumors were seen early in all the imaging studies performed. However, high activity in the kidneys was observed with the radiometal labeled protein. The anti-Her2 affibody has also been labeled with Alexa Fluor for near-infra red imaging. A second affibody molecule against EGFR has also shown successful targeting of tumors in gamma-camera imaging. A clinical pilot study demonstrated that anti-Her2 affibody could delineate tumors as early as 2 hours after administration. Thus it appears that affibody may be favorable molecules as alternative imaging agents.

CONCLUSIONS

It is clear that engineering antibodies for tumor targeting is not a trivial task as several factors regarding the antibody and the target need to be taken into account. For imaging, homogeneous tumor penetration is less important since heterogeneous distribution will still identify the tumor provided that expression of surface molecules is sufficient to discriminate the target tissue from background activity. However, the imaging time frame and radiation exposure to other tissues are governed by specificity and blood clearance of the immunoprobe. Several intact antibodies and to a lesser extent antibody fragments have been evaluated in patients (reviewed in [124–125]). Although preliminary clinical studies with antibody fragment with gamma-camera imaging show encouraging results, to date only intact antibodies have been evaluated by PET. As a result, there is great interest in clinical translation of antibody fragments and alternative affinity scaffolds for tumor targeting with improved properties (i.e. rapid blood clearance), ideal for molecular imaging of surface markers. In addition to enabling early, same day imaging

of malignant lesions that will accelerate evaluation of patient care and treatment, antibody-based molecular imaging tracers will play an important future role in the diagnosis and management of cancer and other diseases.

Acknowledgments

Funding for this work was provided by NIH grants CA 030206, CA 043905, CA 086306, and CA 092131. We thank Dr. James D. Marks for the C6.5 antibody, Dr. Jeffrey V. Leyton for the ^{124}I -C6.5 minibody image and Dr. Vania E. Kenanova for the ^{64}Cu -DOTA-T84.66 scFv-Fc DM image.

REFERENCES

1. Massoud TF, Gambhir SS. Molecular imaging in living subjects: seeing fundamental biological processes in a new light. *Genes Dev* 2003;17:545–580. [PubMed: 12629038]
2. Shreve PD, Anzai Y, Wahl RL. Pitfalls in oncologic diagnosis with FDG PET imaging: physiologic and benign variants. *Radiographics* 1999;19:61–77. quiz 150–151. [PubMed: 9925392]
3. Cai W, Chen X. Multimodality molecular imaging of tumor angiogenesis. *J Nucl Med* 2008;49:113S–128S. [PubMed: 18523069]
4. Tait JF. Imaging of apoptosis. *J Nucl Med* 2008;49:1573–1576. [PubMed: 18794267]
5. Rudin M. Noninvasive imaging of receptor function: signal transduction pathways and physiological readouts. *Curr Opin Drug Discov Devel* 2008;11:606–615.
6. Mankoff DA, Link JM, Linden HM, Sundararajan L, Krohn KA. Tumor receptor imaging. *J Nucl Med* 2008;49:149S–163S. [PubMed: 18523071]
7. Hsiao JK, Law B, Weissleder R, Tung CH. In-vivo imaging of tumor associated urokinase-type plasminogen activator activity. *J Biomed Opt* 2006;11:34013. [PubMed: 16822063]
8. Plathow C, Weber WA. Tumor cell metabolism imaging. *J Nucl Med* 2008;49:43S–63S. [PubMed: 18523065]
9. Kurdziel KA, Kalen JD, Hirsch JI, et al. Imaging multidrug resistance with 4-[^{18}F]fluoropacitaxel. *Nucl Med Biol* 2007;34:823–831. [PubMed: 17921033]
10. Elsinga PH, Hendrikse NH, Bart J, Vaalburg W, van Waarde A. PET Studies on P-glycoprotein function in the blood-brain barrier: how it affects uptake and binding of drugs within the CNS. *Curr Pharm Des* 2004;10:1493–1503. [PubMed: 15134571]
11. Bogdanov A, Weissleder R. *In vivo* imaging of gene delivery and expression. *Trends Biotech* 2002;20:S11–S18.
12. Rosebrough SF, Grossman ZD, McAfee JG, et al. Thrombus imaging with indium-111 and iodine-131-labeled fibrin-specific monoclonal antibody and its F(ab')₂ and Fab fragments. *J Nucl Med* 1988;29:1212–1222. [PubMed: 3392581]
13. Murray JL, Rosenblum MG, Lamki L, et al. Clinical parameters related to optimal tumor localization of indium-111-labeled mouse antimelanoma monoclonal antibody ZME-018. *J Nucl Med* 1987;28:25–33. [PubMed: 3794809]
14. Bird RE, Hardman KD, Jacobson JW, et al. Single-chain antigen-binding proteins. *Science (New York, N.Y)* 1988;242:423–426.
15. Huston JS, Levinson D, Mudgett-Hunter M, et al. Protein engineering of antibody binding sites: recovery of specific activity in an anti-digoxin single-chain Fv analogue produced in *Escherichia coli*. *Proc Natl Acad Sci U S A* 1988;85:5879–5883. [PubMed: 3045807]
16. Wu AM, Senter PD. Arming antibodies: prospects and challenges for immunoconjugates. *Nat Biotechnol* 2005;23:1137–1146. [PubMed: 16151407]
17. Lee JH, Huh YM, Jun YW, et al. Artificially engineered magnetic nanoparticles for ultrasensitive molecular imaging. *Nat Med* 2007;13:95–99. [PubMed: 17187073]
18. Kang JH, Chung JK. Molecular-genetic imaging based on reporter gene expression. *J Nucl Med* 2008;49:164S–179S. [PubMed: 18523072]
19. Merk H, Stiege W, Tsumoto K, Kumagai I, Erdmann VA. Cell-free expression of two single-chain monoclonal antibodies against lysozyme: effect of domain arrangement on the expression. *J Biochem* 1999;125:328–333. [PubMed: 9990130]

20. Kim YJ, Neelamegam R, Heo MA, Edwardraja S, Paik HJ, Lee SG. Improving the productivity of single-chain Fv antibody against c-Met by rearranging the order of its variable domains. *J Microbiol Biotechnol* 2008;18:1186–1190. [PubMed: 1860066]
21. Desplancq D, King DJ, Lawson AD, Mountain A. Multimerization behaviour of single chain Fv variants for the tumour-binding antibody B72.3. *Protein Eng* 1994;7:1027–1033. [PubMed: 7809029]
22. Colcher D, Bird R, Roselli M, et al. In vivo tumor targeting of a recombinant single-chain antigen-binding protein. *J Natl Cancer Inst* 1990;82:1191–1197. [PubMed: 2362290]
23. Nedelman MA, Shealy DJ, Boulin R, et al. Rapid infarct imaging with a technetium-99m-labeled antimyosin recombinant single-chain Fv: evaluation in a canine model of acute myocardial infarction. *J Nucl Med* 1993;34:234–241. [PubMed: 8429342]
24. Milenic DE, Yokota T, Filpula DR, et al. Construction, binding properties, metabolism, and tumor targeting of a single-chain Fv derived from the pancarcinoma monoclonal antibody CC49. *Cancer Res* 1991;51:6363–6371. [PubMed: 1933899]
25. Adams GP, McCartney JE, Tai MS, et al. Highly specific in vivo tumor targeting by monovalent and divalent forms of 741F8 anti-c-erbB-2 single-chain Fv. *Cancer Res* 1993;53:4026–4034. [PubMed: 7689421]
26. Wu AM, Chen W, Raubitschek A, et al. Tumor localization of anti-CEA single-chain Fvs: improved targeting by non-covalent dimers. *Immunotechnology* 1996;2:21–36. [PubMed: 9373325]
27. Pietersz GA, Patrick MR, Chester KA. Preclinical characterization and in vivo imaging studies of an engineered recombinant technetium-99m-labeled metallothionein-containing anti-carcinoembryonic antigen single-chain antibody. *J Nucl Med* 1998;39:47–56. [PubMed: 9443738]
28. George AJ, Jamar F, Tai MS, et al. Radiometal labeling of recombinant proteins by a genetically engineered minimal chelation site: technetium-99m coordination by single-chain Fv antibody fusion proteins through a C-terminal cysteinyl peptide. *Proc Natl Acad Sci U S A* 1995;92:8358–8362. [PubMed: 7667295]
29. Verhaar MJ, Keep PA, Hawkins RE, et al. Technetium-99m radiolabeling using a phage-derived single-chain Fv with a C-terminal cysteine. *J Nucl Med* 1996;37:868–872. [PubMed: 8965166]
30. Waibel R, Alberto R, Willuda J, et al. Stable one-step technetium-99m labeling of His-tagged recombinant proteins with a novel Tc(I)-carbonyl complex. *Nat Biotechnol* 1999;17:897–901. [PubMed: 10471933]
31. Schott ME, Milenic DE, Yokota T, et al. Differential metabolic patterns of iodinated versus radiometal chelated anticarcinoma single-chain Fv molecules. *Cancer Res* 1992;52:6413–6417. [PubMed: 1423290]
32. Reilly RM, Maiti PK, Kiarash R, et al. Rapid imaging of human melanoma xenografts using an scFv fragment of the human monoclonal antibody H11 labelled with ¹¹¹In. *Nucl Med Commun* 2001;22:587–595. [PubMed: 11388583]
33. Choi CW, Lang L, Lee JT, et al. Biodistribution of ¹⁸F- and ¹²⁵I-labeled anti-Tac disulfide-stabilized Fv fragments in nude mice with interleukin 2 alpha receptor-positive tumor xenografts. *Cancer Res* 1995;55:5323–5329. [PubMed: 7585595]
34. Birchler M, Neri G, Tarli L, Halin C, Viti F, Neri D. Infrared photodetection for the in vivo localisation of phage-derived antibodies directed against angiogenic markers. *J Immunol Methods* 1999;231:239–248. [PubMed: 10648941]
35. Ramjiawan B, Maiti P, Aftanas A, et al. Noninvasive localization of tumors by immunofluorescence imaging using a single chain Fv fragment of a human monoclonal antibody with broad cancer specificity. *Cancer* 2000;89:1134–1144. [PubMed: 10964344]
36. Holliger P, Hudson PJ. Engineered antibody fragments and the rise of single domains. *Nat Biotechnol* 2005;23:1126–1136. [PubMed: 16151406]
37. Yang K, Basu A, Wang M, et al. Tailoring structure-function and pharmacokinetic properties of single-chain Fv proteins by site-specific PEGylation. *Protein Eng* 2003;16:761–770. [PubMed: 14600206]
38. Yazaki PJ, Kassa T, Cheung CW, et al. Biodistribution and tumor imaging of an anti-CEA single-chain antibody-albumin fusion protein. *Nucl Med Biol* 2008;35:151–158. [PubMed: 18312824]

39. Yazaki PJ, Wu AM, Tsai SW, et al. Tumor targeting of radiometal labeled anti-CEA recombinant T84.66 diabody and t84.66 minibody: comparison to radioiodinated fragments. *Bioconjug Chem* 2001;12:220–228. [PubMed: 11312683]
40. Goel A, Colcher D, Baranowska-Kortylewicz J, et al. Genetically engineered tetravalent single-chain Fv of the pancarcinoma monoclonal antibody CC49: improved biodistribution and potential for therapeutic application. *Cancer Res* 2000;60:6964–6971. [PubMed: 11156397]
41. Goel A, Baranowska-Kortylewicz J, Hinrichs SH, et al. ^{99m}Tc-labeled divalent and tetravalent CC49 single-chain Fv's: novel imaging agents for rapid in vivo localization of human colon carcinoma. *J Nucl Med* 2001;42:1519–1527. [PubMed: 11585867]
42. King DJ, Turner A, Farnsworth AP, et al. Improved tumor targeting with chemically cross-linked recombinant antibody fragments. *Cancer Res* 1994;54:6176–6185. [PubMed: 7954464]
43. Sheikholvaezin A, Eriksson D, Ahlstrom KR, Johansson L, Stigbrand T. Tumor radioimmunolocalization in nude mice by mono- and divalent- single-chain Fv antiplacental alkaline phosphatase antibodies. *Cancer Biother Radiopharm* 2007;22:64–72. [PubMed: 17627415]
44. Adams GP, McCartney JE, Wolf EJ, et al. Enhanced tumor specificity of 741F8-1 (sFv)², an anti-erbB-2 single-chain Fv dimer, mediated by stable radioiodine conjugation. *J Nucl Med* 1995;36:2276–2281. [PubMed: 8523119]
45. Spooner RA, Murray S, Rowlinson-Busza G, Deonarain MP, Chu A, Epenetos AA. Genetically engineered antibodies for diagnostic pathology. *Hum Pathol* 1994;25:606–614. [PubMed: 8013953]
46. Dubel S, Breitling F, Kontermann R, Schmidt T, Skerra A, Little M. Bifunctional and multimeric complexes of streptavidin fused to single chain antibodies (scFv). *J Immunol Methods* 1995;178:201–209. [PubMed: 7836782]
47. Lin Y, Pagel JM, Axworthy D, Pantelias A, Hedin N, Press OW. A genetically engineered anti-CD45 single-chain antibody-streptavidin fusion protein for pretargeted radioimmunotherapy of hematologic malignancies. *Cancer Res* 2006;66:3884–3892. [PubMed: 16585217]
48. Pagel JM, Lin Y, Hedin N, et al. Comparison of a tetravalent single-chain antibody-streptavidin fusion protein and an antibody-streptavidin chemical conjugate for pretargeted anti-CD20 radioimmunotherapy of B-cell lymphomas. *Blood* 2006;108:328–336. [PubMed: 16556891]
49. Sato N, Hassan R, Axworthy DB, et al. Pretargeted radioimmunotherapy of mesothelin-expressing cancer using a tetravalent single-chain Fv-streptavidin fusion protein. *J Nucl Med* 2005;46:1201–1209. [PubMed: 16000290]
50. Forster GJ, Santos EB, Smith-Jones PM, Zanzonico P, Larson SM. Pretargeted radioimmunotherapy with a single-chain antibody/streptavidin construct and radiolabeled DOTA-biotin: strategies for reduction of the renal dose. *J Nucl Med* 2006;47:140–149. [PubMed: 16391198]
51. Green DJ, Pagel JM, Nemecek ER, et al. Pretargeting CD45 enhances the selective delivery of radiation to hemolymphoid tissues in nonhuman primates. *Blood* 2009;114:1226–1235. [PubMed: 19515724]
52. Paganelli G, Chinol M, Maggiolo M, et al. The three-step pretargeting approach reduces the human anti-mouse antibody response in patients submitted to radioimmunoscintigraphy and radioimmunotherapy. *Eur J Nucl Med* 1997;24:350–351. [PubMed: 9143478]
53. Fan CY, Huang CC, Chiu WC, et al. Production of multivalent protein binders using a self-trimerizing collagen-like peptide scaffold. *FASEB J* 2008;22:3795–3804. [PubMed: 18635738]
54. Sanchez-Arevalo Lobo VJ, Cuesta AM, Sanz L, et al. Enhanced antiangiogenic therapy with antibody-collagen XVIII NC1 domain fusion proteins engineered to exploit matrix remodeling events. *Int J Cancer* 2006;119:455–462. [PubMed: 16477626]
55. Rheinhecker M, Hardt C, Ilag LL, et al. Multivalent antibody fragments with high functional affinity for a tumor-associated carbohydrate antigen. *J Immunol* 1996;157:2989–2997. [PubMed: 8816407]
56. Wang D, Wu GJ, Tan JM, Wang H. Study on p53 tetramerization domain in improving functional affinity and biological activity of antibody. *Zhonghua Yi Xue Za Zhi* 2005;85:479–482. [PubMed: 15854555]
57. Liu M, Wang X, Yin C, et al. Targeting TNF-alpha with a tetravalent mini-antibody TNF-TeAb. *Biochem J* 2007;406:237–246. [PubMed: 17472572]

58. Willuda J, Kubetzko S, Waibel R, Schubiger PA, Zangemeister-Wittke U, Pluckthun A. Tumor targeting of mono-, di-, and tetravalent anti-p185(HER-2) miniantibodies multimerized by self-associating peptides. *J Biol Chem* 2001;276:14385–14392. [PubMed: 11278961]
59. Pack P, Pluckthun A. Miniantibodies: use of amphipathic helices to produce functional, flexibly linked dimeric Fv fragments with high avidity in *Escherichia coli*. *Biochemistry* 1992;31:1579–1584. [PubMed: 1737014]
60. Pluckthun A, Pack P. New protein engineering approaches to multivalent and bispecific antibody fragments. *Immunotechnology* 1997;3:83–105. [PubMed: 9237094]
61. Libyh MT, Goossens D, Oudin S, et al. A recombinant human scFv anti-Rh(D) antibody with multiple valences using a C-terminal fragment of C4-binding protein. *Blood* 1997;90:3978–3983. [PubMed: 9354666]
62. Ventura E, Sassi F, Fossati S, et al. Use of uteroglobin for the engineering of polyvalent, polyspecific fusion proteins. *J Biol Chem* 2009;284:26646–26654. [PubMed: 19632988]
63. Natarajan A, Xiong CY, Gruettner C, DeNardo GL, DeNardo SJ. Development of multivalent radioimmunonanoparticles for cancer imaging and therapy. *Cancer Biother Radiopharm* 2008;23:82–91. [PubMed: 18298332]
64. Weng KC, Noble CO, Papahadjopoulos-Sternberg B, et al. Targeted tumor cell internalization and imaging of multifunctional quantum dot-conjugated immunoliposomes in vitro and in vivo. *Nano Lett* 2008;8:2851–2857. [PubMed: 18712930]
65. Yang L, Mao H, Wang YA, et al. Single chain epidermal growth factor receptor antibody conjugated nanoparticles for in vivo tumor targeting and imaging. *Small* 2009;5:235–243. [PubMed: 19089838]
66. Holliger P, Prospero T, Winter G. "Diabodies": small bivalent and bispecific antibody fragments. *Proc Natl Acad Sci U S A* 1993;90:6444–6448. [PubMed: 8341653]
67. Todorovska A, Roovers RC, Dolezal O, Kortt AA, Hoogenboom HR, Hudson PJ. Design and application of diabodies, triabodies and tetrabodies for cancer targeting. *J Immunol Methods* 2001;248:47–66. [PubMed: 11223068]
68. Dolezal O, Pearce LA, Lawrence LJ, McCoy AJ, Hudson PJ, Kortt AA. ScFv multimers of the anti-neuraminidase antibody NC10: shortening of the linker in single-chain Fv fragment assembled in V (L) to V(H) orientation drives the formation of dimers, trimers, tetramers and higher molecular mass multimers. *Protein Eng* 2000;13:565–574. [PubMed: 10964986]
69. Kelly MP, Lee FT, Tahtis K, et al. Tumor targeting by a multivalent single-chain Fv (scFv) anti-Lewis Y antibody construct. *Cancer Biother Radiopharm* 2008;23:411–423. [PubMed: 18771345]
70. Adams GP, Schier R, McCall AM, et al. Prolonged in vivo tumour retention of a human diabody targeting the extracellular domain of human HER2/neu. *Br J Cancer* 1998;77:1405–1412. [PubMed: 9652755]
71. Wu AM, Williams LE, Zieran L, et al. Anti-carcinoembryonic antigen (CEA) diabody for rapid tumor targeting and imaging. *Tumor Targeting* 1999;4:47–58.
72. Perez L, Ayala M, Pimentel G, et al. A multivalent recombinant antibody fragment specific for carcinoembryonic antigen. *Biotechnol Appl Biochem* 2006;43:39–48. [PubMed: 16101587]
73. Sundaresan G, Yazaki PJ, Shively JE, et al. 124I-labeled engineered anti-CEA minibodies and diabodies allow high-contrast, antigen-specific small-animal PET imaging of xenografts in athymic mice. *J Nucl Med* 2003;44:1962–1969. [PubMed: 14660722]
74. Cai W, Olafsen T, Zhang X, et al. PET imaging of colorectal cancer in xenograft-bearing mice by use of an 18F-labeled T84.66 anti-carcinoembryonic antigen diabody. *J Nucl Med* 2007;48:304–310. [PubMed: 17268029]
75. Contag PR, Olomu IN, Stevenson DK, Contag CH. Bioluminescent indicators in living mammals. *Nat Med* 1998;4:245–247. [PubMed: 9461201]
76. Venisnik KM, Olafsen T, Gambhir SS, Wu AM. Fusion of Gaussia luciferase to an engineered anti-carcinoembryonic antigen (CEA) antibody for in vivo optical imaging. *Mol Imaging Biol* 2007;9:267–277. [PubMed: 17577599]
77. Venisnik KM, Olafsen T, Loening AM, Iyer M, Gambhir SS, Wu AM. Bifunctional antibody-Renilla luciferase fusion protein for in vivo optical detection of tumors. *Protein Eng Des Sel* 2006;19:453–460. [PubMed: 16882674]

78. Nielsen UB, Adams GP, Weiner LM, Marks JD. Targeting of bivalent anti-ErbB2 diabody antibody fragments to tumor cells is independent of the intrinsic antibody affinity. *Cancer Res* 2000;60:6434–6440. [PubMed: 11103810]
79. Gonzalez, Trotter DE.; Manjeshwar, RM.; Doss, M., et al. Quantitation of small-animal (124)I activity distributions using a clinical PET/CT scanner. *J Nucl Med* 2004;45:1237–1244. [PubMed: 15235072]
80. Robinson MK, Doss M, Shaller C, et al. Quantitative immuno-positron emission tomography imaging of HER2-positive tumor xenografts with an iodine-124 labeled anti-HER2 diabody. *Cancer Res* 2005;65:1471–1478. [PubMed: 15735035]
81. Leyton JV, Olafsen T, Sherman MA, et al. Engineered humanized diabodies for microPET imaging of prostate stem cell antigen-expressing tumors. *Protein Eng Des Sel* 2009;22:209–216. [PubMed: 18957406]
82. Schneider DW, Heitner T, Alicke B, et al. In vivo biodistribution, PET imaging, and tumor accumulation of 86Y- and 111In-antimindin/RG-1, engineered antibody fragments in LNCaP tumor-bearing nude mice. *J Nucl Med* 2009;50:435–443. [PubMed: 19223400]
83. Sirk SJ, Olma S, Shen CK, et al. MicroPET imaging of HER2+ tumors using F-18-labeled anti-HER2 diabody. *J Nucl Med* 2009;50:128.
84. Lepin, EJ.; Olma, S.; Wang, M.; Reiter, RE.; Shen, CK.; Wu, AM. ¹⁸F-labeled diabodies for microPET imaging of prostate stem cell antigen (PSCA)-expressing xenografts. Montreal, Quebec, Canada: World Molecular Imaging Congress; 2009.
85. Berndorff D, Borkowski S, Moosmayer D, et al. Imaging of tumor angiogenesis using 99mTc-labeled human recombinant anti-ED-B fibronectin antibody fragments. *J Nucl Med* 2006;47:1707–1716. [PubMed: 17015908]
86. Olafsen T, Cheung CW, Yazaki PJ, et al. Covalent disulfide-linked anti-CEA diabody allows site-specific conjugation and radiolabeling for tumor targeting applications. *Protein Eng Des Sel* 2004;17:21–27. [PubMed: 14985534]
87. Sirk SJ, Olafsen T, Barat B, Bauer KB, Wu AM. Site-specific, thiol-mediated conjugation of fluorescent probes to cysteine-modified diabodies targeting CD20 or HER2. *Bioconjug Chem* 2008;19:2527–2534. [PubMed: 19053310]
88. Barat B, Sirk SJ, McCabe KE, et al. Cys-diabody Quantum Dot Conjugates (ImmunoQdots) for Cancer Marker Detection. *Bioconjug Chem*. 2009
89. Olafsen T, Sirk SJ, Betting DJ, et al. ImmunoPET imaging of B-cell lymphoma using ¹²⁴I-anti-CD20 scFv dimers (diabodies). *Protein Eng Des Sel*. In press.
90. Hu S, Shively L, Raubitschek A, et al. Minibody: A novel engineered anti-carcinoembryonic antigen antibody fragment (single-chain Fv-CH3) which exhibits rapid, high-level targeting of xenografts. *Cancer Res* 1996;56:3055–3061. [PubMed: 8674062]
91. Wu AM, Yazaki PJ, Tsai S, et al. High-resolution microPET imaging of carcinoembryonic antigen-positive xenografts by using a copper-64-labeled engineered antibody fragment. *Proc Natl Acad Sci U S A* 2000;97:8495–8500. [PubMed: 10880576]
92. Leyton JV, Olafsen T, Lepin EJ, et al. Humanized radioiodinated minibody for imaging of prostate stem cell antigen-expressing tumors. *Clin Cancer Res* 2008;14:7488–7496. [PubMed: 19010866]
93. Olafsen T, Kenanova VE, Sundaresan G, et al. Optimizing radiolabeled engineered anti-p185HER2 antibody fragments for in vivo imaging. *Cancer Res* 2005;65:5907–5916. [PubMed: 15994969]
94. Olafsen T, Tan GJ, Cheung CW, et al. Characterization of engineered anti-p185HER-2 (scFv-CH3) 2 antibody fragments (minibodies) for tumor targeting. *Protein Eng Des Sel* 2004;17:315–323. [PubMed: 15187222]
95. Adams GP, Shaller CC, Dadachova E, et al. A single treatment of yttrium-90-labeled CHX-A"-C6.5 diabody inhibits the growth of established human tumor xenografts in immunodeficient mice. *Cancer Res* 2004;64:6200–6206. [PubMed: 15342405]
96. Olafsen T, Gu Z, Sherman MA, et al. Targeting, imaging, and therapy using a humanized antiprostate stem cell antigen (PSCA) antibody. *J Immunother* 2007;30:396–405. [PubMed: 17457214]
97. Olafsen T, Betting D, Kenanova VE, et al. Recombinant anti-CD20 antibody fragments for small-animal PET imaging of B-cell lymphomas. *J Nucl Med* 2009;50:1500–1508. [PubMed: 19690034]
98. Whitlow M, Bell BA, Feng SL, et al. An improved linker for single-chain Fv with reduced aggregation and enhanced proteolytic stability. *Protein Eng* 1993;6:989–995. [PubMed: 8309948]

99. Borsi L, Balza E, Bestagno M, et al. Selective targeting of tumoral vasculature: comparison of different formats of an antibody (L19) to the ED-B domain of fibronectin. *Int J Cancer* 2002;102:75–85. [PubMed: 12353237]
100. Rossin R, Berndorff D, Friebe M, Dinkelborg LM, Welch MJ. Small-animal PET of tumor angiogenesis using a (76)Br-labeled human recombinant antibody fragment to the ED-B domain of fibronectin. *J Nucl Med* 2007;48:1172–1179. [PubMed: 17574989]
101. Tijink BM, Perk LR, Budde M, et al. (124)I-L19-SIP for immuno-PET imaging of tumour vasculature and guidance of (131)I-L19-SIP radioimmunotherapy. *Eur J Nucl Med Mol Imaging* 2009;36:1235–1244. [PubMed: 19259661]
102. Silacci M, Brack SS, Spath N, et al. Human monoclonal antibodies to domain C of tenascin-C selectively target solid tumors in vivo. *Protein Eng Des Sel* 2006;19:471–478. [PubMed: 16928692]
103. Kenanova V, Olafsen T, Crow DM, et al. Tailoring the pharmacokinetics and positron emission tomography imaging properties of anti-carcinoembryonic antigen single-chain Fv-Fc antibody fragments. *Cancer Res* 2005;65:622–631. [PubMed: 15695407]
104. Andersen JT, Justesen S, Fleckenstein B, et al. Ligand binding and antigenic properties of a human neonatal Fc receptor with mutation of two unpaired cysteine residues. *FEBS J* 2008;275:4097–4110. [PubMed: 18637944]
105. Kenanova V, Olafsen T, Williams LE, et al. Radioiodinated versus radiometal-labeled anti-carcinoembryonic antigen single-chain Fv-Fc antibody fragments: optimal pharmacokinetics for therapy. *Cancer Res* 2007;67:718–726. [PubMed: 17234783]
106. Zuckier LS, Chang CJ, Scharff MD, Morrison SL. Chimeric human-mouse IgG antibodies with shuffled constant region exons demonstrate that multiple domains contribute to in vivo half-life. *Cancer Res* 1998;58:3905–3908. [PubMed: 9731501]
107. Alyanakian MA, Bernatowska E, Scherrmann JM, Aucouturier P, Poplavsky JL. Pharmacokinetics of total immunoglobulin G and immunoglobulin G subclasses in patients undergoing replacement therapy for primary immunodeficiency syndromes. *Vox Sang* 2003;84:188–192. [PubMed: 12670367]
108. Valadon P, Garnett JD, Testa JE, Bauerle M, Oh P, Schnitzer JE. Screening phage display libraries for organ-specific vascular immunotargeting in vivo. *Proc Natl Acad Sci U S A* 2006;103:407–412. [PubMed: 16384919]
109. Schmidt MM, Thurber GM, Wittrup KD. Kinetics of anti-carcinoembryonic antigen antibody internalization: effects of affinity, bivalency, and stability. *Cancer Immunol Immunother* 2008;57:1879–1890. [PubMed: 18408925]
110. Hendriks BS, Opresko LK, Wiley HS, Lauffenburger D. Quantitative analysis of HER2-mediated effects on HER2 and epidermal growth factor receptor endocytosis: distribution of homo- and heterodimers depends on relative HER2 levels. *J Biol Chem* 2003;278:23343–23351. [PubMed: 12686539]
111. Ackerman ME, Pawlowski D, Wittrup KD. Effect of antigen turnover rate and expression level on antibody penetration into tumor spheroids. *Mol Cancer Ther* 2008;7:2233–2240. [PubMed: 18645032]
112. Austin CD, De Maziere AM, Pisacane PI, et al. Endocytosis and sorting of ErbB2 and the site of action of cancer therapeutics trastuzumab and geldanamycin. *Mol Biol Cell* 2004;15:5268–5282. [PubMed: 15385631]
113. van Osdol W, Fujimori K, Weinstein JN. An analysis of monoclonal antibody distribution in microscopic tumor nodules: consequences of a "binding site barrier". *Cancer Res* 1991;51:4776–4784. [PubMed: 1893370]
114. Adams GP, Schier R, McCall AM, et al. High affinity restricts the localization and tumor penetration of single-chain fv antibody molecules. *Cancer Res* 2001;61:4750–4755. [PubMed: 11406547]
115. Graff CP, Wittrup KD. Theoretical analysis of antibody targeting of tumor spheroids: importance of dosage for penetration, and affinity for retention. *Cancer Res* 2003;63:1288–1296. [PubMed: 12649189]
116. Adams GP, Schier R, Marshall K, et al. Increased affinity leads to improved selective tumor delivery of single-chain Fv antibodies. *Cancer Res* 1998;58:485–490. [PubMed: 9458094]

117. Schier R, McCall A, Adams GP, et al. Isolation of picomolar affinity anti-c-erbB-2 single-chain Fv by molecular evolution of the complementarity determining regions in the center of the antibody binding site. *J Mol Biol* 1996;263:551–567. [PubMed: 8918938]
118. Rudnick SI, Adams GP. Affinity and avidity in antibody-based tumor targeting. *Cancer Biother Radiopharm* 2009;24:155–161. [PubMed: 19409036]
119. Nuttall SD, Walsh RB. Display scaffolds: protein engineering for novel therapeutics. *Curr Opin Pharmacol* 2008;8:609–615. [PubMed: 18619558]
120. Gebauer M, Skerra A. Engineered protein scaffolds as next-generation antibody therapeutics. *Curr Opin Chem Biol* 2009;13:245–255. [PubMed: 19501012]
121. Huang L, Gaikam LO, Caveliers V, et al. SPECT imaging with ^{99m}Tc-labeled EGFR-specific nanobody for in vivo monitoring of EGFR expression. *Mol Imaging Biol* 2008;10:167–175. [PubMed: 18297364]
122. Cortez-Retamozo V, Lahoutte T, Caveliers V, et al. ^{99m}Tc-Labeled Nanobodies: A New Type of Targeted Probes for Imaging Antigen Expression. *Curr Radiopharm* 2008;1:37–47.
123. Friedman M, Stahl S. Engineered affinity proteins for tumour-targeting applications. *Biotechnol Appl Biochem* 2009;53:1–29. [PubMed: 19341363]
124. van Dongen GA, Visser GW, Lub-de Hooge MN, de Vries EG, Perk LR. Immuno-PET: a navigator in monoclonal antibody development and applications. *Oncologist* 2007;12:1379–1389. [PubMed: 18165614]
125. Wu AM. Antibodies and antimatter: the resurgence of immuno-PET. *J Nucl Med* 2009;50:2–5. [PubMed: 19091888]

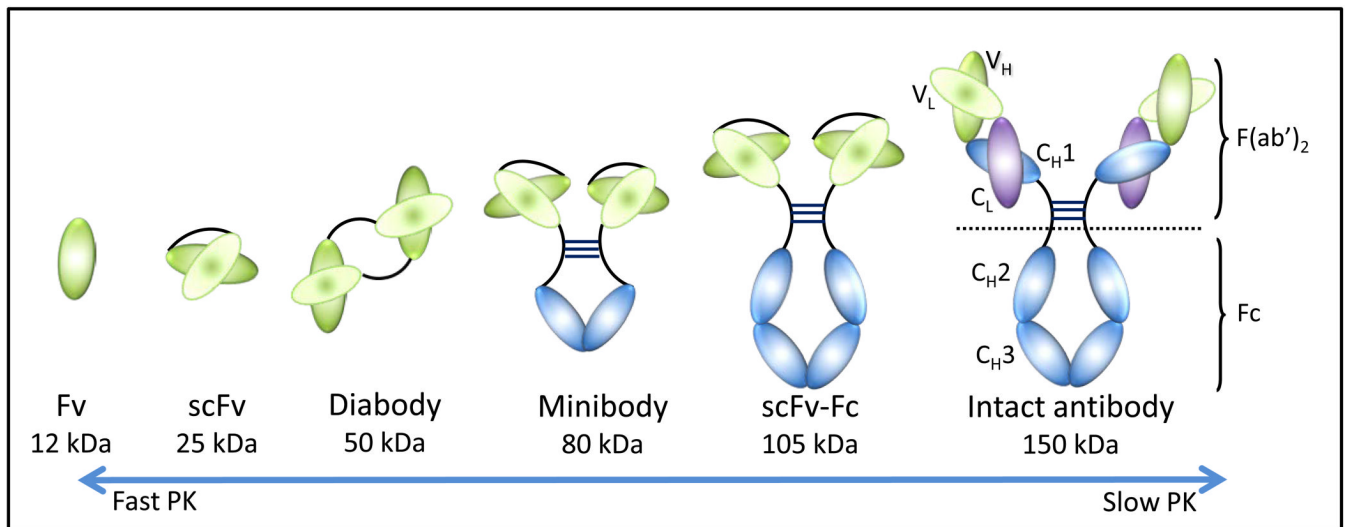


Fig. 1. Schematic presentation of an intact antibody and engineered antibody fragments derived from it including a single variable domain fragment (Fv), single chain Fv (scFv), diabody, minibody and scFv-Fc. Molecular weights are indicated below each fragment. V_L = variable light (light green); V_H = variable heavy (dark green), C_L = constant light (pink); C_H = constant heavy (blue).

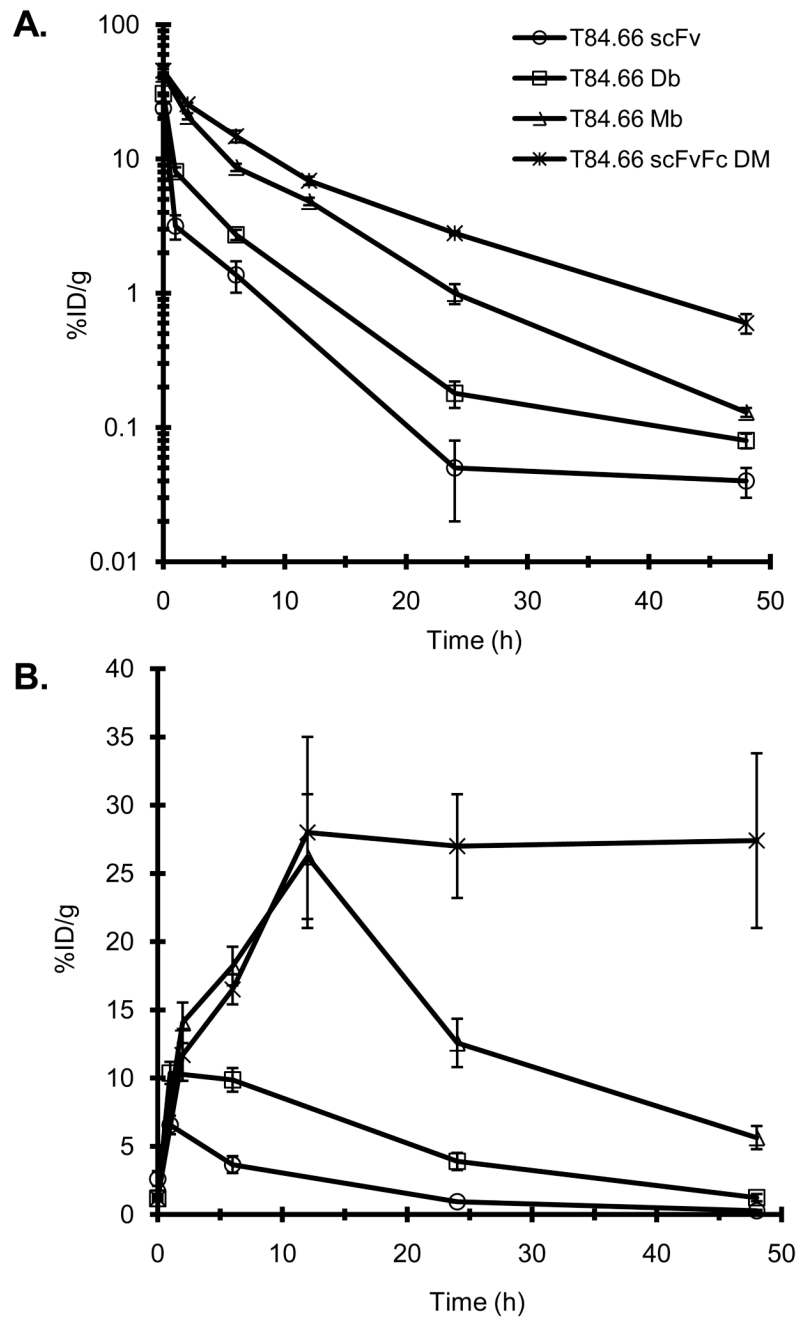


Fig. 2. Blood clearance (A) and tumor uptake (B) curves of radioiodine-labeled anti-CEA T84.66 antibody fragments in mice carrying subcutaneous LS174T human colon carcinoma xenografts. Standard errors are shown. Uptake is expressed as percentage of injected dose per gram (% ID/g). The scFv-Fc fragment, modified to clear quickly by the introduction of two mutations in the Fc region that interfere the FcRn interaction, is referred to as double mutant (DM). The longer persistence of radiolabeled fragments in the circulation leads to higher and more persistent tumor uptakes, but longer times are required to obtain high contrast imaging. Data are from ^{26,39,105}.

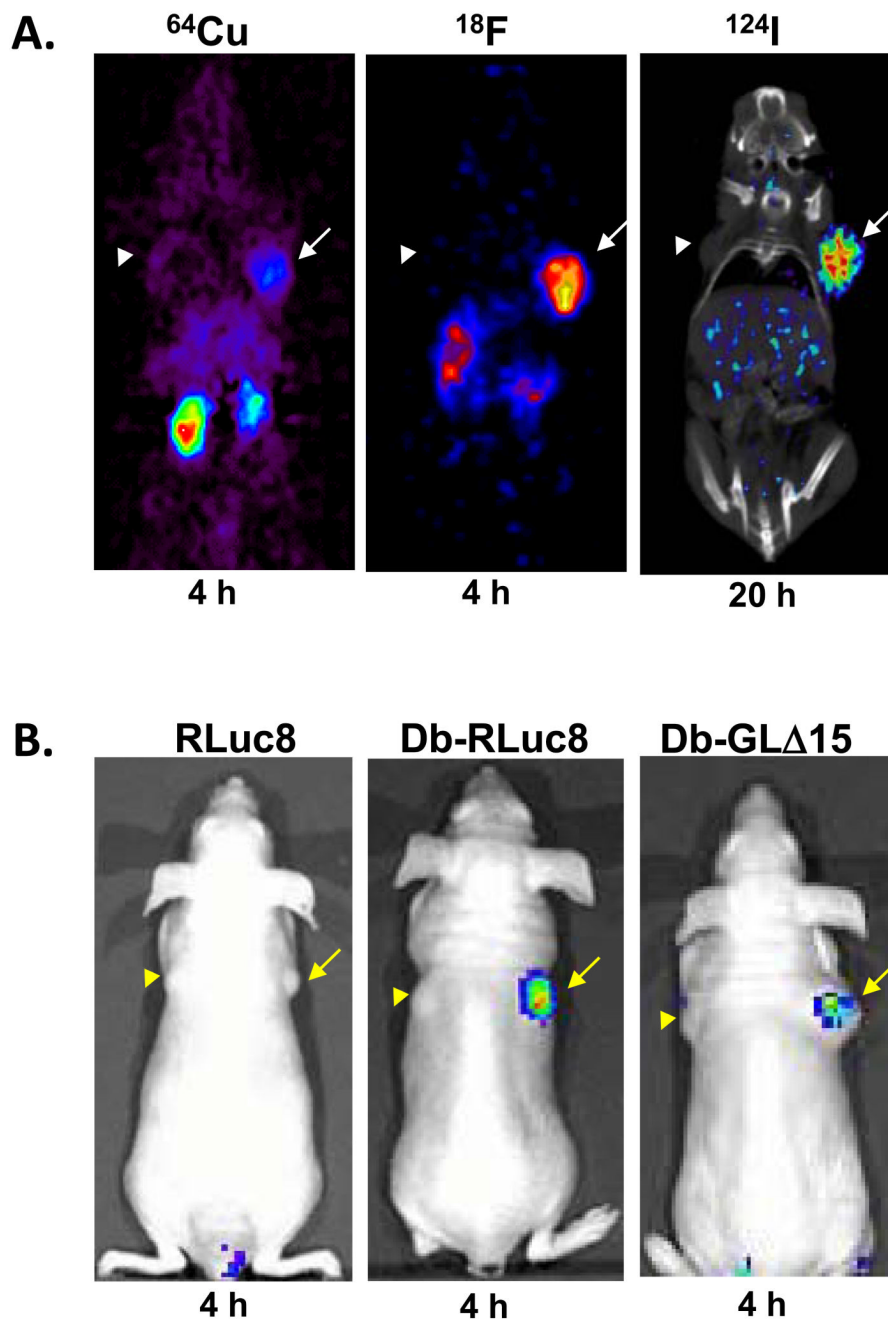


Fig. 3. Small animal PET (A) and optical imaging (B) of anti-CEA T84.66 diabody in LS174T xenograft-bearing mice 73:74:76:77. A. Coronal PET images of mice injected with diabody following radiolabeling with different positron emitting radionuclides. Specific localization to the positive tumor (arrow) and no localization to the negative C6 rat glioma tumors (arrowhead) are seen in all the images. Renal clearance is evident at 4 hours p.i. with ^{64}Cu - and ^{18}F -labeled diabodies which is expected for a fragment of < 60 kDa in size. High contrast imaging is achieved with ^{124}I -labeled diabody at 20 hour p.i. due to almost complete elimination of any background activity, and a PET/CT overlaid image is shown for anatomical reference. B. Bioluminescence imaging of mice injected with diabody-renilla (Db-RLuc8) and -gaussia

(Db-GL Δ 15) luciferase fusion proteins at 4 hours p.i. The control mouse injected with Rluc8 only is shown. Specific targeting to the positive tumor is seen with both fusion proteins.

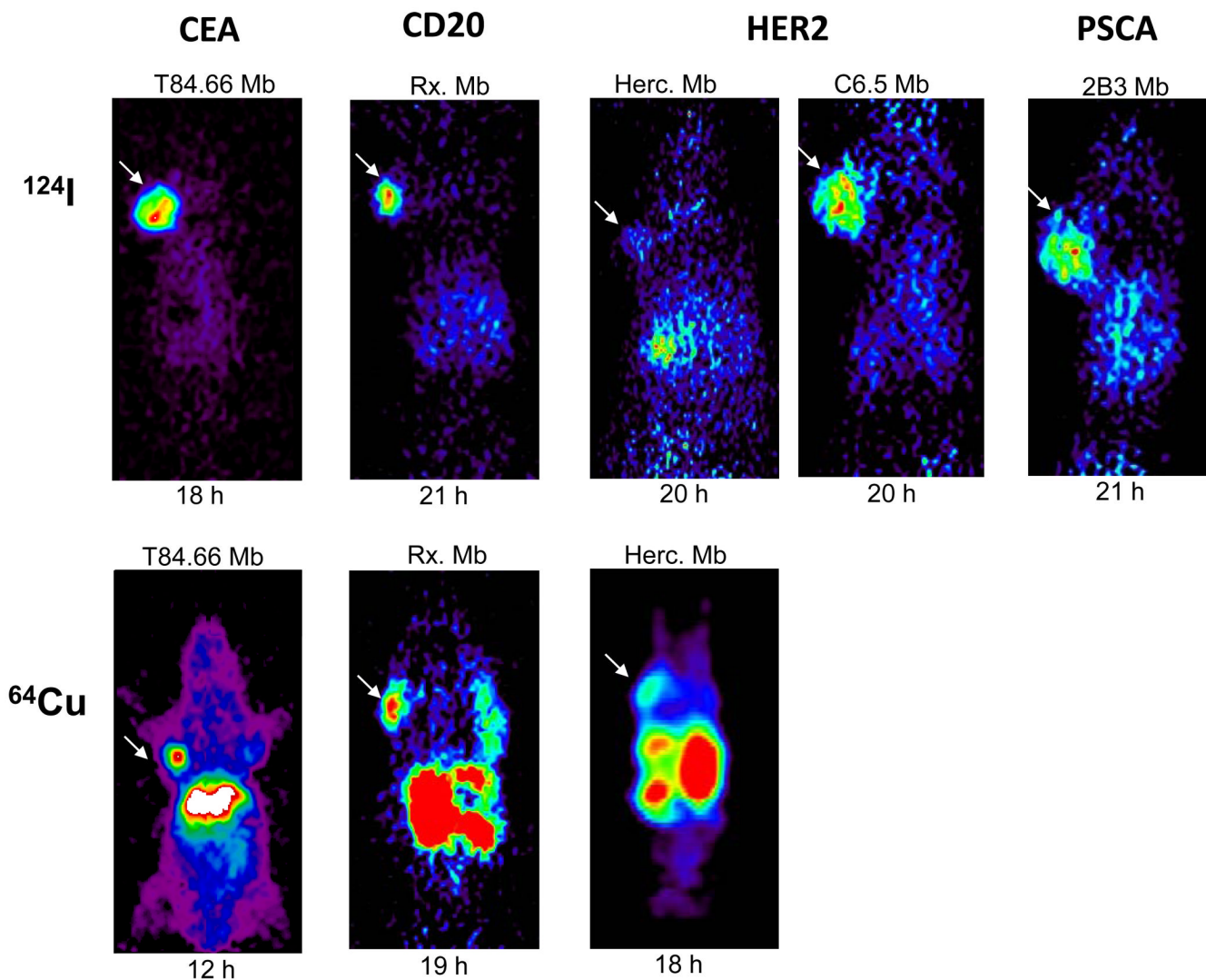


Fig. 4. Small animal PET imaging of xenograft-bearing mice injected with ^{124}I -labeled (top) and ^{64}Cu -DOTA minibodies (bottom) against different cell surface antigens. Minibodies against CEA (T84.66 Mb) 73, CD20 (Rx. Mb) 97, Her2 (Herc. Mb) 93 were radiolabeled and imaged with both radionuclides. The anti-Her2 C6.5 Mb and anti-PSCA 2B3 Mb 92 were radiolabeled with ^{124}I only. All ^{124}I -labeled minibodies, except the ^{124}I -Herc. Mb, produce high contrast images at 18–21 hours p.i. Less contrast is achieved with ^{64}Cu -DOTA minibodies due to high background activity. Hepatic clearance is evident with the ^{64}Cu -DOTA minibodies as expected for a fragment of > 60 kDa in size.

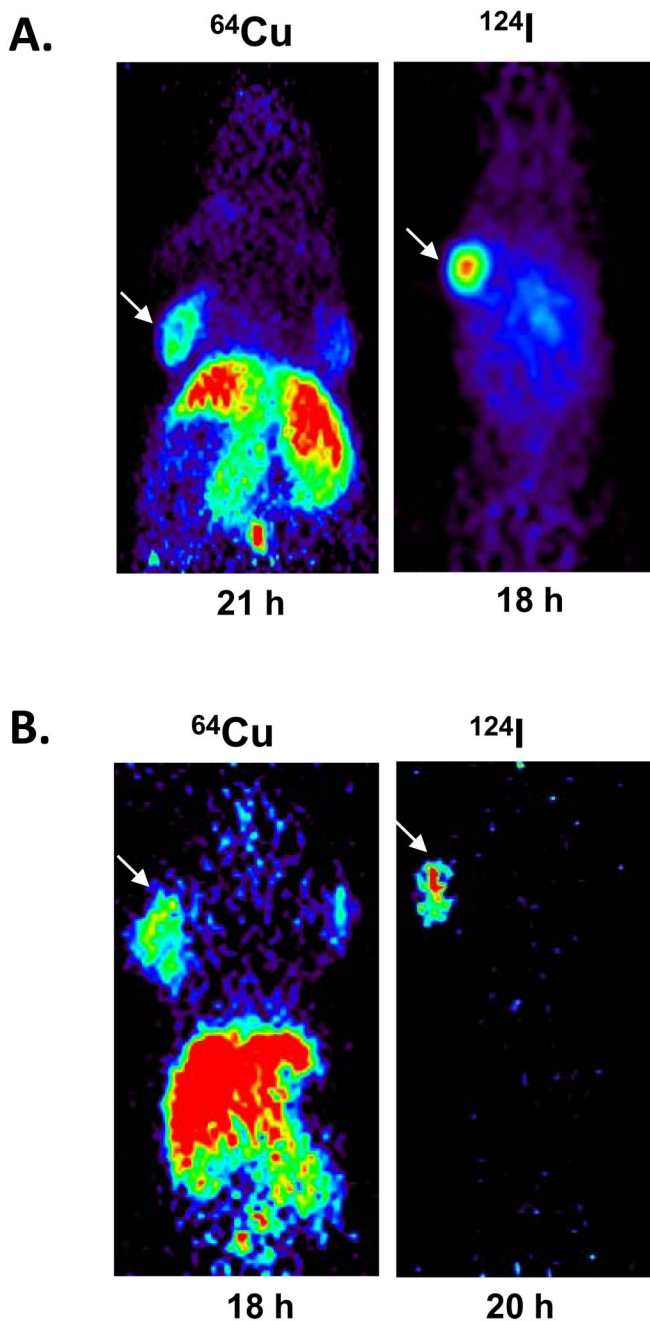


Fig. 5. Small animal PET imaging of xenograft-bearing mice injected with ^{64}Cu and/or ^{124}I -labeled scFv-Fc double mutant (DM) fragments targeting CEA (A) and CD20 (D)^{97,103}. The background activity of ^{124}I -anti-CD20 scFv-Fc with IgG4 Fc is less (1.9% ID/g at 21 hours p.i.)⁹⁷ than that seen with ^{124}I -anti-CEA scFv-Fc with IgG1 Fc region (6.9% ID/g at 12 hours and 2.8% ID/g at 24 hours p.i.)¹⁰⁵, suggesting a more rapid clearance rate of this anti-CD20 fragment. This is consistent with published observation of the different blood clearances of human IgG1 and IgG4 isotypes. Again, ^{64}Cu -labeled fragments produce less contrast than ^{124}I -labeled fragments and hepatic clearance is evident.

TABLE 1

Antibody-based imaging agents in the clinic

Generic name (trade name)	Company	Date of FDA approval	Antibody, format	Target	Radiolabel	Approved indications
Satumomab pendetide* (OncoScint)	Cytogen	December, 1992	B72.3 mouse IgG1	TAG-72	¹¹¹ In	Colorectal and ovarian carcinoma
Arcitumomab (CEA-Scan)	Immunomedics	June, 1996	IMMU-4, mouse IgG1 Fab'	CEA	^{99m} Tc	Colorectal, breast, and small cell lung carcinoma
Imciromab pentetate* (Myoscint)	Centocor	July, 1996	R11D10, mouse IgG2a Fab'	Myosin	¹¹¹ In	Myocardial necrosis
Nofetumomab merpentan (Verluma)	Boehringer Ingelheim	August, 1996	NR-LU-10, mouse IgG2b Fab	40-kDa glycoprotein	^{99m} Tc	Small cell and non-small cell lung carcinoma
Capromab pendetide (ProstaScint)	Cytogen	October, 1996	7E11-C5.3, mouse IgG1	100-kDa glycoprotein	¹¹¹ In	Prostate carcinoma
Ibritumomab tiuxetan (Zevalin)	Spectrum Pharmis	February, 2002	2B8, mouse IgG1	CD20	¹¹¹ In	Non-Hodgkin lymphoma
Tositumomab (Bexxar)	SmithKline Beecham	June, 2003	B1, mouse IgG2a	CD20	¹³¹ I	Non-Hodgkin lymphoma
Fanolesomab* (NeuroSpec former LeuTech)	Palatin Technologies	July, 2004	RB5, mouse IgM	CD15	^{99m} Tc	Appendicitis
Bectumomab (LymphoScan)	Immunomedics	Not in US	LL2, mouse IgG2a Fab'	CD22	^{99m} Tc	Non-Hodgkin lymphoma
Votumumab (HumaSPECT)	Intracel	Not in US	88BY59, human IgG3	Altered cyokeratins	^{99m} Tc	Colorectal, ovarian and breast carcinoma
Igovomab* (Indimacis-125)	CIS Bio International	Not in US	OC125, mouse IgG1 F(ab') ₂	CA-125	¹¹¹ In	Ovarian cancer
Sulesomab (LeukoScan)	Immunomedics	Not in US	IMMU-MN3 mouse IgG1 Fab'	NCA-90	^{99m} Tc	Osteomyelitis, appendicitis, inflammatory bowel disease

* no longer marketed